HHS Public Access

Author manuscript

J Mater Sci Mater Med. Author manuscript; available in PMC 2018 November 28.

Published in final edited form as:

J Mater Sci Mater Med. 2016 August ; 27(8): 125. doi:10.1007/s10856-016-5735-0.

The Characterization of Decellularized Human Skeletal Muscle as a Blueprint for Mimetic Scaffolds

Klaire Wilson[1], **Abby Terlouw**[1], **Kevin Roberts**[2], and **Jeffrey C. Wolchok**[1]

[1]Department of Biomedical Engineering, College of Engineering, University of Arkansas

[2]Cell and Molecular Biology Program, University of Arkansas

Abstract

The use of decellularized skeletal muscle (DSM) as a cell substrate and scaffold for the repair of volumetric muscle loss injuries has shown therapeutic promise. The performance of DSM materials motivated our interest in exploring the chemical and physical properties of this promising material. We suggest that these properties could serve as a blueprint for the development of next generation engineered materials with DSM mimetic properties. In this study, whole human lower limb rectus femoris (n=10) and upper limb supraspinatus muscle samples (n=10) were collected from both male and female tissue donors. Skeletal muscle samples were decellularized and nine property values, capturing key compositional, architectural, and mechanical properties, were measured and statistically analyzed. Mean values for each property were determined across muscle types and genders. Additionally, the influence of muscle type (upper versus lower limb) and donor gender (male versus female) on each of the DSM material properties was examined. The data suggests that DSM materials prepared from lower limb rectus femoris samples have an increased modulus and contain a higher collagen content then upper limb supraspinatus muscles. Specifically, lower limb rectus femoris DSM material modulus and collagen content was approximately twice that of lower limb supraspinatus DSM samples. While muscle type did show some influence on material properties, we did not find significant trends related to gender. The material properties reported herein may be used as a blueprint for the data-driven design of next generation engineered scaffolds with muscle mimetic properties, as well as inputs for computational and physical models of skeletal muscle.

Keywords

skeletal muscle; extracellular matrix; decellularization; volumetric muscle loss

1. Introduction

There are currently few options available to surgeons tasked with the treatment of severely damaged skeletal muscle. Following mild injury (e.g. strains, contusions, and lacerations) muscle tissue has the capacity for self-repair [1, 2] and surgical intervention is not warranted. However, when significant muscle volume (>20%) is damaged or lost (trauma,

Corresponding Author: Jeff Wolchok, 125 Engineering Hall, Department of Biomedical Engineering, University of Arkansas, Fayetteville, AR 72701, jwolchok@uark.edu, 479 575-2850 (phone), 479 575-2846 (fax).

infection, or surgical resection) the regenerative capabilities of muscle are overwhelmed, resulting in the formation of non-contractile scar tissue within the defect site [3]. When faced with this type of injury, termed volumetric muscle loss (VML), the current standard of care is the transfer of autologous muscle flaps, or in many instances no treatment at all. Flap transfers have been used to reconstruct forearm, elbow, and shoulder muscles [4–6]. While often effective, the transfer of healthy autologous muscle tissue is an extremely invasive procedure that causes significant donor site morbidity. Skeletal muscle repair strategies that do not rely on the harvest of autologous tissue warrant exploration.

As an alternative to muscle flap transfer, the use of decellularized skeletal muscle (DSM) scaffolds for the repair of muscle defects has shown promise. Specifically, the implantation of cell seeded DSM scaffolds into VML defects has been shown to promote myogenesis and increase muscle force generation in several small animal models [7]. Decellularized muscle implants are thought to stimulate muscle repair by restoring lost regenerative cues and providing a substrate for muscle progenitor cell (satellite cell) myogenesis [8]. The encouraging outcomes that have been achieved thus far using DSM implants support a guiding principle suggesting that the properties of native muscle extracellular matrix (ECM) provide a positive myogenic environment for transplanted cells during the repair of damaged skeletal muscle. Guided by this principle, the development of readily available “off the shelf” biomaterials with properties that mimic DSM are an attractive adjunct to tissue derived DSM scaffolds. Research groups [9–11], including ours [12] have reported the development of engineered scaffolds with muscle inspired properties.

The accurate recapitulation of the physical and chemical properties of human muscle ECM is an understandable target for those in pursuit of implantable scaffolds with muscle mimetic characteristics. Yet, the application and assessment of DSM biomaterials has been focused primarily on in-vivo host response assays [13, 14], and less so on their key material properties. The objective of this study was to characterize several key chemical and physical properties of DSM prepared from whole human skeletal muscle collected from both upper (supraspinatus) and lower (rectus femoris) extremity muscles. In addition to the collection of skeletal muscle tissue properties, the influence of muscle harvest location (upper versus lower limb) and donor gender (male versus female) on material properties was explored. While location and gender influence the size and physiology of whole muscle tissue, it is not known whether harvest location and donor gender significantly influences the properties of the ECM and by extension the DSM collected from skeletal muscle. From the perspective of the tissue engineer or biomaterial scientist interested in scaffold development, these differences may be of interest. If only minor differences are detected between muscle location and donor gender, it would suggest that a single set of measured parameters could be used to develop a universal design template that closely recapitulates human muscle ECM. However, if significant differences are detected, then this might suggest that location and gender specific engineered implants may need to be considered.

While our goal is the creation of a muscle ECM blueprint, the increased exploration of decellularized tissues by various research groups [15–18] certainly suggests that DSM biomaterials might serve an important clinical role. Potentially, as has been shown with commercially available bladder and intestinal derived biomaterials, the ECM derived from

skeletal muscle may find utility for applications beyond muscle repair. When one considers that tissue banks rarely if ever collect human muscle tissue, its untapped potential as an additional source of implantable ECM is attractive. Towards this end, the careful cataloging of skeletal muscle ECM properties, like that described in this study, may help identify suitable future applications for this material while location and gender differences could help influence donor selection criteria. More broadly, these values would add to the growing library of decellularized tissue properties available to biomaterial scientists and computational modelers. To sum, the results from this study will provide a comprehensive set of skeletal muscle ECM material values that could be used to not only guide the development of muscle mimetic biomaterial scaffolds, but also allow potential users to asses the suitability of DSM as a surgical repair material.

2. Materials and Methods

2.1 Overview of experimental design

Whole human rectus femoris (n=10; 5 male / 5 female) and supraspinatus (n=10; 5 male / 5 female) skeletal muscle samples were procured from a commercial tissue donation center (Science Care, Phoenix, AZ). Skeletal muscle samples were decellularized using a published [19] SDS-based decellularization protocol [19] familiar to our group and previously used to prepare rat DSM samples [12, 20]. The resulting ECM biomaterial was thoroughly characterized to determine several key physical and chemical properties. Characterization tests included:

1. ECM yield (g ECM / g whole muscle)
2. Collagen content (% wet weight),
3. Glycosaminoglycan (GAG) content (% wet weight)
4. Modulus of elasticity (kPa)
5. Porosity (%)
6. Network Alignment (degrees)
7. Tandem mass spectrometry (qualitative protein fingerprint)
8. ATR-FTIR spectroscopy (chemical bond fingerprint)
9. Degradation rate (% volume loss / week)

Whole and decellularized skeletal muscle sample architecture, surface appearance and composition were qualitatively characterized using a panel of imaging techniques. The influence of muscle harvest location (upper versus lower limb) and gender (male versus female) on each of the key parameters was evaluated.

2.2 Decellularization

Upon arrival, the rectus femoris (RF) and supraspinatus (SS) muscles were stored at - 80°C. In preparation for decellularization, frozen whole muscle samples were thawed, cleaned of any residual fat and tendon, weighed, imaged, sectioned into strips or plugs, and batch decellularized. Samples were soaked in 1% sodium dodecyl sulfate (SDS) with 1% EDTA in

Tris-HCL buffer (pH 8.0) for approximately two weeks at room temperature using gentle agitation and multiple decellularization solution exchanges. To remove nuclear remnants, samples were incubated for 12 hours at 4C in a reaction buffer containing 1 kU/ml DNase/RNase. Samples were rinsed in PBS (pH 7.4) for approximately 48 hours (4C) to remove any residual decellularization solutions between each preparation step. ECM yield for each sample was calculated as the ratio of decellularized sample weight (g) to pre-decellularization whole muscle sample weight (g). Yield for each samples was measured in triplicate. Once decellularized, the hydrated samples were either immediately utilized or frozen (−80C) until needed for testing

2.3 Imaging

Representative whole and decellularized skeletal muscle samples were sectioned with the aid of a cryostat (CM1860, Leica Biosystems, Buffalo Grove, IL.). Samples were fixed in 4% paraformaldehyde, sectioned to a thickness of 15um and mounted on microscopic slides. Mounted sections were permeabilized with 0.1% Triton X-100 and blocked with 4% goat serum. Slides were immuno-reacted for the presence of collagen type 1 (Sigma-Aldrich, 1:500), chondroitin sulfate proteoglycans (Sigma-Aldrich, dilution 1:500), and cytoskeletal actin, (Invitrogen, 1:50 dilution), followed by incubation in the appropriate fluorescently labeled secondary antibodies (Alexa 488 and 594, Invitrogen,1:500). Sections were counterstained with the nuclear dye DAPI and then microscopically imaged. Additionally, representative whole and decellularized muscle samples were lyophilized, sputter coated with platinum, and imaged with the aid of a scanning electron microscope.

2.4 Porosity and Orientation

Decellularized RF and SS samples were incubated in 10% formalin overnight at 4°C, paraffin embedded and sectioned in either the transverse (across muscle fibers) or longitudinal (along muscle fibers) direction with the aid of a microtome (5um). Sections were mounted on microscopic slides, stained with hematoxylin and eosin (H&E), and microscopically imaged (100X). Two representative images, taken from difference tissue regions within each sample (n = 8 / muscle type, 4 male and 4 female) were used to measure porosity (% open space) and ECM network alignment (dominant orientation angle) using image analysis software (ImageJ) and guided by published techniques [21, 22] used previously by our group [23]. Porosity and alignment were measured from transverse and longitudinally sectioned samples respectively. The direction of muscle contraction (long axis of the RF and SS muscles) was selected to correspond to an orientation angle of 0 degrees. The measurement of dominant orientation angles close to 0 degrees is indicative of network alignment in the direction of contraction, while 90 degrees would suggest perpendicularity.

2.5 Biochemical Assessment

Decellularized RF and SS sample collagen content (% dry weight) was estimated from hydroxy-proline concentration. Hydroxyproline concentration was determined from extracted samples (n = 8 / muscle type, 4 male and 4 female) using a published technique [24]. Briefly, extracted samples were digested in a 6N HCL solution (20 hrs at 115°C) and then neutralized with sodium hydroxide. Digested samples were mixed with a chloramine T solution (1:2) and incubated at room temperature for 20 minutes. A dimethyl-

aminobenzaldehyde assay solution was added (1:2) and the mixture was incubated at 65°C for 25 minutes. During this time a red chromophore develops. Chromophore intensity indicates hydroxy-proline concentration. Sample absorbance was read at 570 nm using a microplate reader. RF and SS values were compared against a standard curve, and collagen concentrations were calculated. Samples were tested in triplicate.

Glycosaminoglycan concentrations of human RF and SS ECM samples (n = 8 / muscle type, 4 male and 4 female) were determined with the Blyscan Sulfated Glycosaminoglycan Assay Kit (Biocolor Ltd., Carrickfergus, Co Antrium, United Kingdom). Briefly, samples were digested using a papain extraction reagent method. Samples were digested at a concentration of 30–40 mg (wet weight) per 1.5 ml of papain reagent at 65°C for 3 hours. Digested samples and standards were treated with Blyscan dye reagent then treated with dissociation reagent. Samples and standards were run in triplicate on a ninety-six well plate and read at an absorbance of 656 nm.

2.6 Mechanical Testing

In preparation for mechanical testing, RF and SS muscle sample (n = 8 / muscle type; 4 male and 4 female) were thawed at room temperature and sectioned into 3 cm X 0.5 cm strips aligned in the direction of muscle contraction. Uniaxial tensile testing was accomplished with the aid of a computer controlled material testing system (5944, Instron, Norwood, MA) incorporating a 10N load cell. Manufacturer software (Bluehill Lite, Instron, Norwood, MA) was used to control strain rate and record force/elongation data. The long axis of hydrated samples (PBS) was aligned in the direction of loading and secured at each end using hand tightened serrated grips. A gauge length of 2 cm was used for all samples. Two DSM tissue strips were tested for each sample and then averaged. Prior to tensile testing, samples were preconditioned using 5 cycles of 10% strain to establish a uniform loading history for all samples. Immediately following pre-conditioning, each sample was loaded to failure at a quasi-static strain rate of 10 mm/min. Raw data was collected at a sampling rate of 10 Hz. For each tissue sample, engineering stress versus strain curves were generated from load and elongation data. From these curves, the secant moduli were calculated at 10% strain

2.7 ATR-FTIR and Tandem Mass Spectroscopy

The infrared absorbance spectrum was assessed for both rectus femoris and supraspinatus DSM samples using Fourier transform infrared spectroscopy (FTIR). Infrared spectra were obtained by FTIR in attenuated total reflection mode (Perkin Elmer). RF and SS samples were analyzed in the 900 to 1800 cm^{-1} range with a resolution of 8 cm^{-1}. FTIR spectra were examined for the presence of amine bond absorbance peaks and compared between muscle types. To more broadly determine the proteomic composition, representative rectus femoris and supraspinatus DSM samples were analyzed with tandem mass spectroscopy (MS/MS). Each sample was washed with 50 mM ammonium bicarbonate, denatured (Protease Max, Promega, Madison, WI) for 30 minutes at room temperature, trypsin (20 ng/μl) digested overnight at 37°C, and purified (Ziptip, Milipore, Billerica, MA). The MS/MS analysis was performed under the direction of the University of Utah proteomics core facility using a hybrid mass spectrometer (LTQ-FT, Thermo Scientific, Waltham, MA). Primary peptide molecular mass spectra were acquired by Fourier transform ion cyclotron resonance. The

sequencing of individual peptide spectra was performed by collision induced dissociation in the linear ion trap. Sample proteins were identified by comparison of MS/MS measured peptide sequences to a trypsin-cut specific protein database (Mascot ver. 2.2.1, Matrix Science Inc., Boston, MA).

2.8 In-vivo Degradation

In-vivo degradation was examined using a dorsal subcutaneous implant site in a mouse model. In-vivo degradation was assayed at short-term (4 weeks), mid-term (8 weeks), and longer term (16 weeks) time points (n = 4 / time point). Male outbred mice (CD1, Harlan, Indianapolis IN) were used for all time points tested. All surgical procedures were performed in accordance with protocols approved by the University of Arkansas Institutional Animal Care and Use Committee (IACUC #12026). Anesthesia was induced via IP injection of a ketamine/xylazine cocktail. The subcutaneous implant site was surgically exposed through a 2 cm left-right incision placed 2 finger widths caudal to the scapulae. A subcutaneous pouch was created in each animal by blunt dissection. A single DSM disk (approximate size 9.5 mm x 3 mm) prepared from decellularized RF muscle was implanted into each pouch. Incisions were closed using surgical adhesive (VetBond, 3M). Following surgery all animals were housed in the University of Arkansas Central Laboratory Animal Facility.

At the prescribed time-points (4, 8, and 16 weeks) all animals were euthanized via inhalation of carbon dioxide. The implant site with surrounding soft tissue was harvested and imaged. Implants with the surrounding soft tissue were fixed in 4% paraformaldehyde, paraffin embedded, sectioned with the aid of a microtome, and representative sections were imaged. Using both implant site and histological images, implant diameter and thickness was measured and used to calculate implant volume. Changes in implant volume with time were used as a metric of DSM degradation.

2.8 Data Analysis

All data is presented as the mean ± the standard error of the mean, except for the ages and weights of each sample, which is presented as mean ± standard deviation. The yield, collagen content, GAG content, elastic modulus at 10% strain, porosity, and orientation angle were all analyzed with a two factor (muscle type and gender) analysis of variance (ANOVA). Post hoc comparisons were made using Tukey’s test. A standard 0.05 level of significance was used for all statistical tests. The half-life was determined from an exponential curve fit to the DSM pellet degradation data. Age, height, and body mass difference between genders was evaluated with a two sided Student’s t-test. Significance was reported for $P < 0.05$ for all data. All ANOVA analyses were performed using JMP software (JMP Statistical Discovery from SAS, Cary, NC).

3. Results

The average age (n=20) of all skeletal muscle tissue donors at the time of death was 69.8± 6.6 years. Female and male donor ages were 65.6±5.8 and 74.0±6.0 years respectively. Donor ages ranged from a low of 24 years (male) to a high of 98 years

(female). Although on average male donors were older (8.4 years) than female donors, no statistically significant differences in donor age were detected between genders ($p<0.05$). Similarly, rectus femoris tissue donors (70.0±5.8) were older than supraspinatus donors (65.8±7.2), yet the age difference (4.2 years) between was not statistically significant. Skeletal muscle tissue donor demographic data is summarized in Table 1.

The average mass of whole muscle rectus femoris samples (73.1±12.5g) was approximately 300% greater than supraspinatus muscle (25.4±2.5g) samples (Figure 1). The difference in mass between muscle types was statistically different ($p<0.01$). Female skeletal muscle samples were on average significantly smaller than male muscle samples for both rectus femoris (34% smaller) and supraspinatus muscle (42% smaller) samples. The difference in muscle weight detected between genders was consistent with the significant difference in height detected between genders. On average, female donors were 10% shorter than male muscle donors, yet average body mass index between the two genders was not significantly different.

Prior to decellularization, both rectus femoris and supraspinatus muscle samples were characterized by a deep crimson color consistent with the presence of intracellular myoglobin. Intracellular myoglobin, as well as actin and nuclear remnants were visible within whole muscle sections (Figure 2). Following two weeks of 1% SDS incubation, all samples utilized for subsequent characterization experiments had transitioned from opaque red to a translucent off-white color consistent with the appearance of decellularized facial muscle described by others [14]. Representative decellularized skeletal muscle samples (examined for each muscle type) were no longer immuno-reactive to either myoglobin or actin. Furthermore, DAPI-positive cell nuclei could not be qualitatively detected within images collected from decellularized tissue sections and quantitative DNA values (4.8±0.5 ug/mg of decellularized tissue) were well below the concentration threshold (50–70 ug/mg) reported by others [25, 26].

On average, 20.3±2.6 mg (dry weight) of ECM was collected for every gram (wet weight) of whole muscle following decellularization. Rectus femoris and supraspinatus samples yielded 21.4±3.9 mg and 19.1±3.7 mg of ECM respectively (Figure 3). Average ECM yield was not significantly different between muscle types. Average female muscle ECM yields were consistently higher for both rectus femoris (61% greater) and supraspinatus (25% greater) samples, however the difference between male and femoale was not statistically significant. The range between the lowest (8.0 mg) and highest yielding samples (39.8 mg) was five-fold, suggesting a notable amount of variability between donors.

When viewed in both longitudinal and transverse cross sections, all decellularized muscle samples were characterized by a porous yet interconnected network, with pore locations consistent with the location of once-present muscle cells (Figure 4). Both rectus femoris and supraspinatus samples were highly porous with average porosities of 79±5% and 74±3% respectively. Porosity values ranged from a low of 43% to a high of 88%. No differences in average porosity were detected between muscle types or genders. When viewed longitudinally, sectioned samples (Figure 5) showed evidence of material network alignment in the direction of muscle contraction (defined as zero degrees). The dominant orientation

angle averaged across all samples was 12.±1.4 degrees. The orientation angle was within 16 degrees of the direction of contraction for all samples tested. Orientation angle values ranged from a high of 16 degrees to a low of 6 degrees. No differences in network alignment were detected between muscle types, however the average orientation angle measured from male rectus femoris samples was significantly closer to the direction of contraction (7.6±1.4 degrees) when compared to female rectus femoris values (11.4±0.7 degrees). Similar differences were not observed in supraspinatus female and male samples (12±1.8 degrees versus 15±4.7 degrees).

Both rectus femoris and supraspinatus samples were strongly immunoreactive to antibodies directed against collagen type 1 and CSPG (Figure 6). The average collagen content for all samples was 21.1% of material dry weight, and range from a low of 9% to a high of 32%. The collagen content of rectus femoris samples (28.7±5.7%) was twice as high supraspinatus samples (13.6±1.9%). The difference was statistically significant. No differences in collagen composition were detected between genders. The sGAG content average across all samples was 4.3±0.3% or approximately 20% of the collagen content. No statistically significant differences were detected when gender and muscle type were examined. sGAG concentrations for all samples tested ranged from a low of 2.1% to a high of 5.7%.

Decellularized skeletal muscle samples were durable and amenable to handling and tensile testing. Stress-strain curves were characterized by a short toe-in region (out to about 5%) followed by a nearly linear increase in stress extending out to failure which occurred at approximately 75–125% (Figure 7). Similar stress versus strain patterns were observed for each sample tested. The average tan modulus at 10% strain was 218±41 kPa for all muscle types and genders combined. The tan modulus at 10% strain ranged from a low of 50 kPa (male supraspinatus) to a high of 527 kPa (female rectus femoris). The average rectus femoris elastic modulus was significantly greater than supraspinatus samples. On average, the rectus femoris tan modulus (299±50 kPa) was 95% greater than supraspinatus muscle (157±48 kPa) samples. No significant differences in samples modulus were detected between genders.

Absorbance spectra for rectus femoris and supraspinatus DSM samples contained distinct peaks at locations that are indicative of primary, secondary, and tertiary amines within the ATR-FTIR spectra of all samples (Figure 8). Similar peaks have been observed within the ATR-FTIR spectra of human tissues including articular cartilage [27, 28]. There were no notable differences in the spectra between samples. Eighteen extracellular matrix proteins were identified within material samples using tandem mass spectrometry. The structural ECM proteins that were identified included both fibrillar (type I, III), and fibrillar associated (type IV, VI and XII) collagens, as well as the structural proteoglycans decorin, biglycan, and lumican. Several multifunctional matrix glycoproteins were also identified including the cell adhesive proteins fibronectin and laminin. The pro-angiogenic growth factor vascular endothelial growth factor was also identified within DSM samples.

All animals tolerated the implantation surgery well and gained weight at a rate (0.8 g/week) that was consistent with control animals. The average implant volume (mm^3) was calculated

at 4, 8, and 16 weeks using measurements obtained from gross surface (implant diameter) and historical cross section (implant thickness) images (Figure 9). All animals reached their respective implantation endpoints without complication (n=4 / endpoint). At four weeks, implanted ECM pellets were well incorporated and clearly visible within the subcutaneous space. While signs of mild active inflation could be observed (redness surrounding the implant), there were no signs of tissue necrosis or exudate (pus) accumulation at the implant site. At 4 weeks, implanted pellets had lost on average 67% of their pre-implantation volume. By eight and sixteen weeks, implant volume was further reduced to 92% and 97% respectively, when compared to pre-implantation volume. At sixteen weeks, residual implant fragments were observed in 3 of the 4 animals. The implant could not be detected in 1 animal. The implant volume degradation profile was well described by exponential decay (R^2=0.92). From the exponential decay curve fit, an implant half-life of 2.9 weeks was calculated. A summary of all DSM properties collected is provided in Table 2.

4. Discussion:

Over the past decade, a steady shift has refocused development efforts away from synthetic scaffolds and towards scaffolds derived from decellularized tissues that can be remodeled by the body's own wound healing machinery [29–32]. Their biomimetic composition and architecture gives these naturally derived biomaterials a level of complexity and remodelability not observed with synthetic materials [33, 34]. To our knowledge, the DSM data measured in this study is the first to explore and compare the larger muscles of the extremities as well as gender effects. The DSM materials prepared during the course of this study were collected with the goal of providing a quantitative set of muscle specifications that would help guide the development of next generation scaffolds with muscle mimetic properties. However, the DSM material itself has qualities that appear make it a suitable implant for tissue repair and augmentation. When considering the potential clinical use of DSM materials, the findings of this study indicate that human muscle, although cell-dense, can be thoroughly decellularized, removing both intracellular proteins and DNA, to create robust scaffolds. By all indications, the material is rich with ECM molecules, porous, organized, and sufficiently robust to withstand surgical handling and implantation. When combined with the subcutaneous implantation results that indicate DSM is readily biodegradable through natural wound repair mechanics, the collective findings support future investigation of DSM therapeutic applications.

The selection of the key properties explored in this study is not exhaustive, but do capture the fundamental mechanical, compositional, architectural, and biodegradation properties of native skeletal muscle ECM. In additional to guiding scaffold development, these properties could also prove to be of value to groups interested in the development of skeletal muscle computational models including recent growth and remodeling approaches that utilize tissue ECM parameters during model development and validation [35]. The data could also be used to help guide the development of physical models. Realistic shoulder cuff or lower limb models could be used as hands-on training aids for health care providers learning arthroscopic shoulder procedures or trauma repair techniques. It is generally difficult to provide live human training experiences; as a result it is common during the early training

period to utilize realistic anatomical models [36]. We believe a realistic model that incorporates actual tissue properties could have significant clinical utility as a training tool.

The selection of the rectus femoris and supraspinatus muscle samples collected form the lower and upper extremities respectively, was motivated by the anticipated clinical target for future muscle regenerative scaffolds. In recent military conflicts involving American military personnel the majority of injuries that required hospitalization and transport from the theater involved orthopedic injuries to the extremities. While advances in body armor have significantly improved torso and head protection, the exposed extremities remain vulnerable to the effects of improvised explosive devices and other battlefield explosives. The most severe injuries present in the form of blast injuries, which typically involve the destruction of large segments of bone, muscle, tendon, cartilage, and other musculoskeletal tissues. The definitive care of these devastating blast injuries both in the acute and now chronic setting would benefit from regenerative biomaterials that can repair or replace musculoskeletal tissues lost to trauma. As the military evolves, and the participation of female soldiers in combat situations increases, an improved understanding of how gender may affect musculoskeletal tissue properties could prove valuable.

The development of shoulder muscle regenerative scaffolds would have broad utility within the general population. Degeneration of shoulder muscle is a significant contributor to shoulder cuff surgery failure. The standard surgical treatment for damaged rotator cuffs (400,000 surgeries / year) is reattachment of the torn tendon(s) to their original bony insertion sites on the humerus. Despite significant progress with arthroscopic techniques and improved fixation devices, rotator cuff surgery failure rates, reported to be around 30–35%, remain troublingly high [37–39]. The pathological degeneration of shoulder muscle that occurs in patients with rotator cuff tears is a contributing factor to the high failure rate [40]. The muscles of the rotator cuff undergo progressive and predictable fatty degeneration (also termed fatty infiltration) following tendon tear [41, 42]. While traditional devices (sutures and suture anchors) and biologics have been developed to address the torn tendonous portion of the damaged rotator cuff, there are currently no effective methods to regenerate fatty infiltrated muscle. Fatty infiltration is a well-recognized but currently unaddressed pathological condition that limits the success of rotator cuff surgery [43–45]. Reconstruction of rotator cuff muscle using muscle flap transfers has been considered, but not yet performed to our knowledge, likely out of concern for the morbidity that would result. Clinically, we envision a surgical approach wherein the damaged muscle belly would be reconstructed using a muscle regenerative implant. To our knowledge there have been no attempts to develop materials targeting the reconstruction of damaged rotator cuff muscles. Even a modest reduction to the failure rate could eliminate tens of thousands of repeat procedures and greatly reduce rotator cuff related health care expenses.

While female whole muscles samples were on average significantly smaller than male muscles, a finding that is consistent with known gender differences in muscle mass [46], gender did not significantly influence most of the key DSM properties measured in this study (alignment was significantly different). Although not statistically significant, there were gender related trends that warrant discussion. Namely, for both supraspinatus and rectus femoris samples the DSM yield was greater for female subjects. Female skeletal

muscle yielded, on average, 40% more DSM than male samples, potentially suggesting a denser ECM network within female patients. This finding is consistent with our data indicating that female DSM samples were less porous than male samples, although the differences were not statistically significant. Published data indicating that female muscle fiber diameter is smaller than males may also help explain a finding of increased yield [47]. The smaller, more densely packed muscle fibers in females would correspond to a more densely packed network of ECM sheaths that surround each fiber. The lack of gender specific differences, would suggest certain properties of muscle ECM have such critical importance that they are conserved between genders. Among the properties explored, the alignment and composition of DSM showed the most consistency between male and female samples. Average dominant orientation angle and compositional values (collagen and sGAG) for male and female samples were each within 25% of each other. Of note, this is the first study we are aware of to explore gender differences for human decellularized tissue biomaterials. While we found no significant differences, it may be valuable to know whether gender differences exist for other decellularized tissues.

The alignment in the direction of contraction measured for both muscle types and across gender is not by itself unexpected, but as previously mentioned suggests the physiological importance of alignment and supports the exploration of ECM network alignment as a key factor within the design of muscle mimetic regenerative scaffolds We, as well as others, anticipate that scaffolds with muscle mimetic network alignment will improve muscle regeneration by providing the appropriate topographical cues during healing [48, 49]. In whole muscle, ECM surrounds and supports multinucleated myofibers which are highly aligned in the direction of muscle contraction. The individual fibers range from 5 to 100 um in diameter, and can be as long as several centimeters [50]. In-vitro models indicate that muscle progenitor cells utilize alignment cues during myogenesis [51, 52]. Similar alignment-sensitive responses have been reported for other cells, including cardiac muscle and tendons [53, 54]. Yet, while the many in-vitro alignment studies support the motivation of aligned regenerative scaffolds, we recognize that in-vivo evidence indicating that scaffold alignment is critical to muscle implant success does not exist. The lack of in-vivo data supporting the importance of scaffold alignment in muscle regenerative therapies would appear to motivate future studies.

The effect of muscle location on each of the key material properties was observed as differences in DSM modulus of elasticity and collagen content. On average, rectus femoris samples were twice as stiff and contained twice as much collagen as upper extremity supraspinatus samples. The relationship between collagen content and moduli seems logical, as collagen is a key load-bearing and force-resisting ECM constituent within musculoskeletal tissues. The large forces that are generated by the weight-bearing muscles of the lower extremity may explain the modulus differences we measured. During exercise these forces can exceed several thousand newtons [55]. It may also point to differences in the displacements that each muscle must undergo during shoulder and knee joint motion. The decreased moduli recorded for supraspinatus muscle could be necessary to accommodate the complex multi-degree of freedom rotations that the shoulder joint undergoes during movement and in particular during overhead activities in which the

tendons and muscles of the shoulder cuff impinge upon the acromial arch [56]. Under these punishing physiological conditions increased tissue compliance may help avoid injury.

The average DSM modulus values for both muscle types tested in this study fall below the values reported for other decellularized tissue scaffolds, including commercially available porcine intestinal and bladder tissue [57, 58], but are similar to values reported for facial DSM material [14]. The importance of accurately matching scaffold modulus values to native muscle tissue during VML repair has not been investigated, but in-vitro studies have shown that muscle progenitor cells sense and respond to substrate stiffness. Muscle progenitor cell myogenesis is significantly enhanced when grown on soft substrate and reduced on stiff substrates [59, 60]. Similar cell-substrate stiffness interactions have been noted for other cells including cardiomyocytes [61]. The DSM moduli values measured in this study are on average an order of magnitude below the values reported for common degradable scaffolding materials including PLGA and PCL [62]. This would suggest that if substrate stiffness is an important myogenic factor, then these traditional materials when used as scaffolding might not maximize myogenic potential.

While often explored for synthetic polymers, the degradation rate of ECM scaffolds is frequently overlooked. Understanding the degradation rate of a scaffolding material is meaningful in light of research that suggests that degradation rate can influence regeneration [63]. In this study, the in-vivo degradation rate of the human skeletal ECM, measured as the half-life, was evaluated using a subcutaneous implant in a mouse model. The degradation rate of human muscle ECM samples measured in this study (2.9 weeks) appears closely tuned to the regeneration rate observed for healing skeletal muscle following injury. In separate animal model experiments, groups have shown that following muscle injury, new myofibers repopulate about 25% of the injured area at two weeks and up to 75% at four weeks [64, 65]. While it is not clear whether the degradation rate of subcutaneously implanted muscle ECM, the value measured in this study, is an accurate predictor of degradation when implanted into a muscle defect, it does provide a comparative baseline value for future muscle regenerative materials. What is notable are the differences in degradation rate between the muscle ECM and common synthetic degradables. Pure PGA and PLGA copolymers scaffolds degrade quickly in-vivo, with half-lives under two weeks, while PCL polymers degrade very slowly, taking several years to degrade [66, 67]. When taken as a whole, the steady degradation of the skeletal muscle pellet observed in this study suggests that it is amenable to remodeling via the body’s own wound healing machinery.

The age of the tissue donors utilized in this study may have influenced the quality of the DSM collected. The advanced age of the tissue donors (average age = 70 years) used in this study is a common limitation associated with studies that utilize donated human tissue. Most young donors meet the criteria for transplantable tissue donation and therfore research tissue collected from young donors is exceeeding rare. So while the age limitation is difficult to avoid, it is improtant to understand how age may affect the properties of the ECM collected from human skeletal muscle. Like most tissues, skeletal muscle is known to change with age. A noticable change is an overall decrease in muscle mass as we age. As human age, skeletal muscle fibers begin to decrease in diamater [68] a conditional termed sarcopenia. As a result, muscle cross sectional area and overall muscle mass decreases with age. The

decrease in overall muscle mass would most likely influence the ECM content within each muscle, potentially resulting in less available ECM from older donors when compared to younger donors. In addition to overall changes in mass, aging has also been shown to increase both the elastic modulus and collagen content of muscle ECM [69, 70]. These age related changes would suggest that the modulus values and collagen values we measured may overestimate the propeties of DSM samples collected from younger donors.

The range of values observed for each of the properties was often large. For example, four-fold differences were measured between the high and low collagen content within the male rectus femoris sample group, whereas average differences between males and females as a whole were more modest (20%). Overall, this certainly seems to suggest that differences observed between individuals within a sample group exceed the differences observed between populations within sample groups. This is common within human data, suggesting patient-specific, rather than population-specific, tissue properties need to be considered if the guiding principle about the importance of mimetic scaffolds is valid. The concepts of personalized medicine has become central to the rethinking of cancer treatment and varous other medical therapies [71, 72] and could similalry become important within the field of regenerative medicine.

We also recognize that the in-vivo regeneration of skeletal muscle involves several cell types, including macrophages and interstitial fibroblast cells, that have the ability to degrade and remodel an implantable scaffold [73, 74]. From that viewpoint, it has been postulated that the material properties at the time of implant need not mimic muscle since the body has the ability to reorganize the matrix to the desired final state. This may be true, as others have reported succesful muscle repair using decellularized tissue other than muscle, including significant work by Badylak and his group [9, 75]. We recognize this possibility and present this data not to displace alternative muscle regeneration strategies, but instead to provide a starting point for the development of adjunct materials. In light of the challenges that still exist for the sucessful treatment of VML injury, the exploration of multiple repair strategies is still warranted.

5. Conclusions

The key findings of this study suggest that:

1. Decellularized muscle materials are robust with and contain a rich assortment of ECM proteins.
2. Donor gender did not broadly affect the key DSM material properties measured in this study.
3. DSM material prepared from lower limb muscles (rectus femoris) was less elastic and more enriched in collagen than materials prepared from upper limb muscles (supraspinatus).
4. DSM materials prepared from both locations and genders were highly aligned in the direction of contractile force generation.

5. DSM materials biodegrade at a rate that is consistent with the reported regeneration of damaged muscle.

6. These findings are the first to extensively explore the key chemical and physical properties of human DSM materials prepared from extremity muscles. This novel data could help guide the data-driven development of next generation VML regenerative materials with muscle mimetic properties.

Acknowledgments:

Research reported in this publication was supported by the National Institute Of Arthritis And Musculoskeletal And Skin Diseases of the National Institutes of Health under Award Number R15AR064481 and the Arkansas Biosciences Institute.

6. References:

[1]. Hill M, Wernig A, Goldspink G. Muscle satellite (stem) cell activation during local tissue injury and repair. J Anat 2003;203:89–99. [PubMed: 12892408]

[2]. Mauro A Satellite cell of skeletal muscle fibers. J Biophys Biochem Cytol 1961;9:493–5. [PubMed: 13768451]

[3]. Terada N, Takayama S, Yamada H, Seki T. Muscle repair after a transsection injury with development of a gap: an experimental study in rats. Scand J Plast Reconstr Surg Hand Surg 2001;35:233–8. [PubMed: 11680391]

[4]. Terzis JK, Kostopoulos VK. Free muscle transfer in posttraumatic plexopathies: part 1: the shoulder. Ann Plast Surg 2010;65:312–7. [PubMed: 20733367]

[5]. Vekris MD, Beris AE, Lykissas MG, Korompilias AV, Vekris AD, Soucacos PN. Restoration of elbow function in severe brachial plexus paralysis via muscle transfers. Injury 2008;39 Suppl 3:S15–22. [PubMed: 18687429]

[6]. Oishi SN, Ezaki M. Free gracilis transfer to restore finger flexion in Volkmann ischemic contracture. Tech Hand Up Extrem Surg 2010;14:104–7. [PubMed: 20526164]

[7]. Merritt EK, Cannon MV, Hammers DW, Le LN, Gokhale R, Sarathy A, et al. Repair of traumatic skeletal muscle injury with bone-marrow-derived mesenchymal stem cells seeded on extracellular matrix. Tissue Eng Part A 2010;16:2871–81. [PubMed: 20412030]

[8]. Grasman JM, Zayas MJ, Page RL, Pins GD. Biomimetic scaffolds for regeneration of volumetric muscle loss in skeletal muscle injuries. Acta Biomater 2015;25:2–15. [PubMed: 26219862]

[9]. Bian W, Bursac N. Engineered skeletal muscle tissue networks with controllable architecture. Biomaterials 2009;30:1401–12. [PubMed: 19070360]

[10]. Chiron S, Tomczak C, Duperray A, Laine J, Bonne G, Eder A, et al. Complex interactions between human myoblasts and the surrounding 3D fibrin-based matrix. PLoS One 2012;7:e36173. [PubMed: 22558372]

[11]. Juhas M, Engelmayr GC, Jr., Fontanella AN, Palmer GM, Bursac N. Biomimetic engineered muscle with capacity for vascular integration and functional maturation in vivo. Proceedings of the National Academy of Sciences of the United States of America 2014;111:5508–13. [PubMed: 24706792]

[12]. Hurd SA, Bhatti NM, Walker AM, Kasukonis BM, Wolchok JC. Development of a biological scaffold engineered using the extracellular matrix secreted by skeletal muscle cells. Biomaterials 2015;49:9–17. [PubMed: 25725550]

[13]. Porzionato A, Sfriso MM, Pontini A, Macchi V, Petrelli L, Pavan PG, et al. Decellularized Human Skeletal Muscle as Biologic Scaffold for Reconstructive Surgery. International journal of molecular sciences 2015;16:14808–31. [PubMed: 26140375]

[14]. Wang L, Johnson JA, Chang DW, Zhang Q. Decellularized musculofascial extracellular matrix for tissue engineering. Biomaterials 2013;34:2641–54. [PubMed: 23347834]

[15]. Kim BS, Choi JS, Kim JD, Choi YC, Cho YW. Recellularization of decellularized human adipose-tissue-derived extracellular matrix sheets with other human cell types. Cell Tissue Res 2012;348:559–67. [PubMed: 22447167]

[16]. Hoenicka M, Schrammel S, Bursa J, Huber G, Bronger H, Schmid C, et al. Development of endothelium-denuded human umbilical veins as living scaffolds for tissue-engineered small-calibre vascular grafts. J Tissue Eng Regen Med 2012.

[17]. Shanti RM, Ziccardi VB. Use of decellularized nerve allograft for inferior alveolar nerve reconstruction: a case report. J Oral Maxillofac Surg 2011;69:550–3. [PubMed: 21145638]

[18]. Evans DW, Moran EC, Baptista PM, Soker S, Sparks JL. Scale-dependent mechanical properties of native and decellularized liver tissue. Biomech Model Mechanobiol 2012.

[19]. Mirsadraee S, Wilcox HE, Korossis SA, Kearney JN, Watterson KG, Fisher J, et al. Development and characterization of an acellular human pericardial matrix for tissue engineering. Tissue Eng 2006;12:763–73. [PubMed: 16674290]

[20]. Wolchok JC, Tresco PA. The isolation of cell derived extracellular matrix constructs using sacrificial open-cell foams. Biomaterials 2010.

[21]. Huang NF, Lee RJ, Li S. Engineering of aligned skeletal muscle by micropatterning. American journal of translational research 2010;2:43–55. [PubMed: 20182581]

[22]. Liu B, Qu M-J, Qin K-R, Li H, Li Z-K, Shen B-R, et al. Role of cyclic strain frequency in regulating the alignment of vascular smooth muscle cells in vitro. Biophysical journal 2008;94:1497–507. [PubMed: 17993501]

[23]. Hurd SA, Bhatti NM, Walker AM, Kasukonis BM, Wolchok JC. Development of a biological scaffold engineered using the extracellular matrix secreted by skeletal muscle cells. Biomaterials 2015;49:9–17. [PubMed: 25725550]

[24]. Edwards CA, O'Brien WD. Modified assay for determination of hydroxyproline in a tissue hydrolyzate. Clinica chimica acta 1980;104:161–7.

[25]. Crapo PM, Gilbert TW, Badylak SF. An overview of tissue and whole organ decellularization processes. Biomaterials 2011;32:3233–43. [PubMed: 21296410]

[26]. Zhang Y, He Y, Bharadwaj S, Hammam N, Carnagey K, Myers R, et al. Tissue-specific extracellular matrix coatings for the promotion of cell proliferation and maintenance of cell phenotype. Biomaterials 2009;30:4021–8. [PubMed: 19410290]

[27]. West PA, Bostrom MP, Torzilli PA, Camacho NP. Fourier transform infrared spectral analysis of degenerative cartilage: an infrared fiber optic probe and imaging study. Appl Spectrosc 2004;58:376–81. [PubMed: 15104805]

[28]. David-Vaudey E, Burghardt A, Keshari K, Brouchet A, Ries M, Majumdar S. Fourier Transform Infrared Imaging of focal lesions in human osteoarthritic cartilage. Eur Cell Mater 2005;10:51–60; discussion [PubMed: 16307426]

[29]. Ott HC, Matthiesen TS, Goh SK, Black LD, Kren SM, Netoff TI, et al. Perfusion-decellularized matrix: using nature's platform to engineer a bioartificial heart. Nat Med 2008;14:213–21. [PubMed: 18193059]

[30]. Yoo JJ, Meng J, Oberpenning F, Atala A. Bladder augmentation using allogenic bladder submucosa seeded with cells. Urology 1998;51:221–5. [PubMed: 9495701]

[31]. Seguin A, Radu D, Holder-Espinasse M, Bruneval P, Fialaire-Legendre A, Duterque-Coquillaud M, et al. Tracheal replacement with cryopreserved, decellularized, or glutaraldehyde-treated aortic allografts. Ann Thorac Surg 2009;87:861–7. [PubMed: 19231406]

[32]. Wainwright JM, Hashizume R, Fujimoto KL, Remlinger NT, Pesyna C, Wagner WR, et al. Right ventricular outflow tract repair with a cardiac biologic scaffold. Cells Tissues Organs 2012;195:159–70. [PubMed: 22025093]

[33]. Hoganson DM, Owens GE, O'Doherty EM, Bowley CM, Goldman SM, Harilal DO, et al. Preserved extracellular matrix components and retained biological activity in decellularized porcine mesothelium. Biomaterials 2010;31:6934–40. [PubMed: 20584548]

[34]. Kim MS, Ahn HH, Shin YN, Cho MH, Khang G, Lee HB. An in vivo study of the host tissue response to subcutaneous implantation of PLGA- and/or porcine small intestinal submucosa-based scaffolds. Biomaterials 2007;28:5137–43. [PubMed: 17764737]

[35]. Ateshian GA, Humphrey JD. Continuum mixture models of biological growth and remodeling: past successes and future opportunities. Annual review of biomedical engineering 2012;14:97–111.

[36]. Lateef F What's new in emergencies, trauma, and shock? Role of simulation and ultrasound in acute care. J Emerg Trauma Shock 2008;1:3–5. [PubMed: 19561934]

[37]. Jost B, Pfirrmann CW, Gerber C, Switzerland Z. Clinical outcome after structural failure of rotator cuff repairs. J Bone Joint Surg Am 2000;82:304–14. [PubMed: 10724223]

[38]. Harryman DT, 2nd, Mack LA, Wang KY, Jackins SE, Richardson ML, Matsen FA, 3rd. Repairs of the rotator cuff. Correlation of functional results with integrity of the cuff. J Bone Joint Surg Am 1991;73:982–9. [PubMed: 1874784]

[39]. Klepps S, Bishop J, Lin J, Cahlon O, Strauss A, Hayes P, et al. Prospective evaluation of the effect of rotator cuff integrity on the outcome of open rotator cuff repairs. Am J Sports Med 2004;32:1716–22. [PubMed: 15494338]

[40]. Goutallier D, Postel JM, Lavau L, Bernageau J. [Impact of fatty degeneration of the suparspinatus and infraspinatus msucles on the prognosis of surgical repair of the rotator cuff]. Rev Chir Orthop Reparatrice Appar Mot 1999;85:668–76. [PubMed: 10612130]

[41]. Gerber C, Schneeberger AG, Hoppeler H, Meyer DC. Correlation of atrophy and fatty infiltration on strength and integrity of rotator cuff repairs: a study in thirteen patients. J Shoulder Elbow Surg 2007;16:691–6. [PubMed: 17931904]

[42]. Gerber C, Meyer DC, Schneeberger AG, Hoppeler H, von Rechenberg B. Effect of tendon release and delayed repair on the structure of the muscles of the rotator cuff: an experimental study in sheep. J Bone Joint Surg Am 2004;86-A:1973–82. [PubMed: 15342760]

[43]. Zumstein MA, Jost B, Hempel J, Hodler J, Gerber C. The clinical and structural long-term results of open repair of massive tears of the rotator cuff. J Bone Joint Surg Am 2008;90:2423–31. [PubMed: 18978411]

[44]. Gerber C, Fuchs B, Hodler J. The results of repair of massive tears of the rotator cuff. J Bone Joint Surg Am 2000;82:505–15. [PubMed: 10761941]

[45]. Di Schino M, Augereau B, Nich C. Does open repair of anterosuperior rotator cuff tear prevent muscular atrophy and fatty infiltration? Clin Orthop Relat Res 2012;470:2776–84. [PubMed: 22733186]

[46]. Roelofs EJ, Smith-Ryan AE, Melvin MN, Wingfield HL, Trexler ET, Walker N. Muscle size, quality, and body composition: characteristics of division I cross-country runners. Journal of strength and conditioning research / National Strength & Conditioning Association 2015;29:290–6.

[47]. Miller AE, MacDougall JD, Tarnopolsky MA, Sale DG. Gender differences in strength and muscle fiber characteristics. European journal of applied physiology and occupational physiology 1993;66:254–62. [PubMed: 8477683]

[48]. Bian W, Bursac N. Engineered skeletal muscle tissue networks with controllable architecture. Biomaterials 2009;30:1401–12. [PubMed: 19070360]

[49]. Lam MT, Huang YC, Birla RK, Takayama S. Microfeature guided skeletal muscle tissue engineering for highly organized 3-dimensional free-standing constructs. Biomaterials 2009;30:1150–5. [PubMed: 19064284]

[50]. Maier F, Bornemann A. Comparison of the muscle fiber diameter and satellite cell frequency in human muscle biopsies. Muscle Nerve 1999;22:578–83. [PubMed: 10331356]

[51]. Jana S, Leung M, Chang J, Zhang M. Effect of nano- and micro-scale topological features on alignment of muscle cells and commitment of myogenic differentiation. Biofabrication 2014;6:035012. [PubMed: 24876344]

[52]. Patel A, Mukundan S, Wang W, Karumuri A, Sant V, Mukhopadhyay SM, et al. Carbon-based hierarchical scaffolds for myoblast differentiation: Synergy between nano-functionalization and alignment. Acta Biomater 2016.

[53]. English A, Azeem A, Spanoudes K, Jones E, Tripathi B, Basu N, et al. Substrate topography: A valuable in vitro tool, but a clinical red herring for in vivo tenogenesis. Acta Biomater 2015;27:3–12. [PubMed: 26318365]

[54]. Morez C, Noseda M, Paiva MA, Belian E, Schneider MD, Stevens MM. Enhanced efficiency of genetic programming toward cardiomyocyte creation through topographical cues. Biomaterials 2015;70:94–104. [PubMed: 26302234]

[55]. Albracht K, Arampatzis A. Influence of the mechanical properties of the muscle-tendon unit on force generation in runners with different running economy. Biological cybernetics 2006;95:87–96. [PubMed: 16628449]

[56]. Brossmann J, Preidler KW, Pedowitz RA, White LM, Trudell D, Resnick D. Shoulder impingement syndrome: influence of shoulder position on rotator cuff impingement--an anatomic study. AJR American journal of roentgenology 1996;167:1511–5. [PubMed: 8956588]

[57]. Dahms SE, Piechota HJ, Dahiya R, Lue TF, Tanagho EA. Composition and biomechanical properties of the bladder acellular matrix graft: comparative analysis in rat, pig and human. British journal of urology 1998;82:411–9. [PubMed: 9772881]

[58]. Tottey S, Johnson SA, Crapo PM, Reing JE, Zhang L, Jiang H, et al. The effect of source animal age upon extracellular matrix scaffold properties. Biomaterials 2011;32:128–36. [PubMed: 20870285]

[59]. Morrissey JB, Cheng RY, Davoudi S, Gilbert PM. Biomechanical Origins of Muscle Stem Cell Signal Transduction. Journal of molecular biology 2015.

[60]. Rao N, Grover GN, Vincent LG, Evans SC, Choi YS, Spencer KH, et al. A co-culture device with a tunable stiffness to understand combinatorial cell-cell and cell-matrix interactions. Integrative biology : quantitative biosciences from nano to macro 2013;5:1344–54. [PubMed: 24061208]

[61]. Ribeiro AJ, Ang YS, Fu JD, Rivas RN, Mohamed TM, Higgs GC, et al. Contractility of single cardiomyocytes differentiated from pluripotent stem cells depends on physiological shape and substrate stiffness. Proceedings of the National Academy of Sciences of the United States of America 2015;112:12705–10. [PubMed: 26417073]

[62]. Baker SC, Rohman G, Southgate J, Cameron NR. The relationship between the mechanical properties and cell behaviour on PLGA and PCL scaffolds for bladder tissue engineering. Biomaterials 2009;30:1321–8. [PubMed: 19091399]

[63]. Tukmachev D, Forostyak S, Koci Z, Zaviskova K, Vackova I, Vyborny K, et al. Injectable Extracellular Matrix Hydrogels as Scaffolds for Spinal Cord Injury Repair. Tissue engineering Part A 2016;22:306–17. [PubMed: 26729284]

[64]. Bibikova A, Oron U. Promotion of muscle regeneration in the toad (Bufo viridis) gastrocnemius muscle by low-energy laser irradiation. The Anatomical record 1993;235:374–80. [PubMed: 8430907]

[65]. Weiss N, Oron U. Enhancement of muscle regeneration in the rat gastrocnemius muscle by low energy laser irradiation. Anatomy and embryology 1992;186:497–503. [PubMed: 1443657]

[66]. Lam CX, Hutmacher DW, Schantz JT, Woodruff MA, Teoh SH. Evaluation of polycaprolactone scaffold degradation for 6 months in vitro and in vivo. Journal of biomedical materials research Part A 2009;90:906–19. [PubMed: 18646204]

[67]. Lu L, Peter SJ, Lyman MD, Lai HL, Leite SM, Tamada JA, et al. In vitro and in vivo degradation of porous poly(DL-lactic-co-glycolic acid) foams. Biomaterials 2000;21:1837–45. [PubMed: 10919687]

[68]. Frontera WR, Zayas AR, Rodriguez N. Aging of human muscle: understanding sarcopenia at the single muscle cell level. Physical medicine and rehabilitation clinics of North America 2012;23:201–7, xiii. [PubMed: 22239884]

[69]. Gao Y, Kostrominova TY, Faulkner JA, Wineman AS. Age-related changes in the mechanical properties of the epimysium in skeletal muscles of rats. Journal of biomechanics 2008;41:465–9. [PubMed: 18031752]

[70]. Wood LK, Kayupov E, Gumucio JP, Mendias CL, Claflin DR, Brooks SV. Intrinsic stiffness of extracellular matrix increases with age in skeletal muscles of mice. Journal of applied physiology 2014;117:363–9. [PubMed: 24994884]

[71]. Matthews PM. Decade in review-multiple sclerosis: new drugs and personalized medicine for multiple sclerosis. Nature reviews Neurology 2015;11:614–6.

[72]. Ziegler A, Koch A, Krockenberger K, Grosshennig A. Personalized medicine using DNA biomarkers: a review. Human genetics 2012;131:1627–38. [PubMed: 22752797]

[73]. Karalaki M, Fili S, Philippou A, Koutsilieris M. Muscle regeneration: cellular and molecular events. In vivo 2009;23:779–96. [PubMed: 19779115]

[74]. Sciorati C, Clementi E, Manfredi AA, Rovere-Querini P. Fat deposition and accumulation in the damaged and inflamed skeletal muscle: cellular and molecular players. Cellular and molecular life sciences : CMLS 2015;72:2135–56. [PubMed: 25854633]

[75]. Sicari BM, Rubin JP, Dearth CL, Wolf MT, Ambrosio F, Boninger M, et al. An acellular biologic scaffold promotes skeletal muscle formation in mice and humans with volumetric muscle loss. Science translational medicine 2014;6:234ra58.

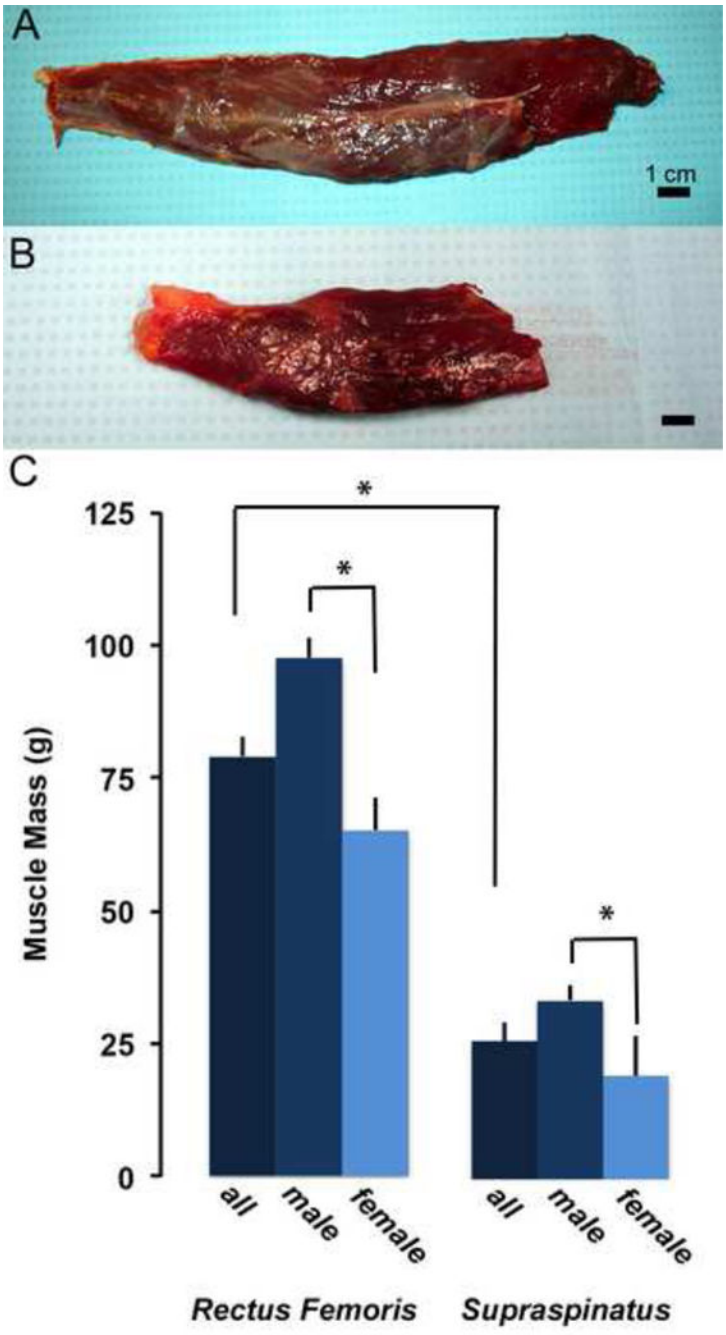

Figure 1:
Representative whole human rectus femoris (A) and supraspinatus (B) muscle samples. Lower extremity rectus femoris muscles were approximately 5 times (The manuscript says 3, the graph looks closer to 3) the mass of shoulder cuff supraspinatus muscles (C). Both rectus femoris and supraspinatus muscles collected from female donors were approximately two-thirds the mass of male muscles.

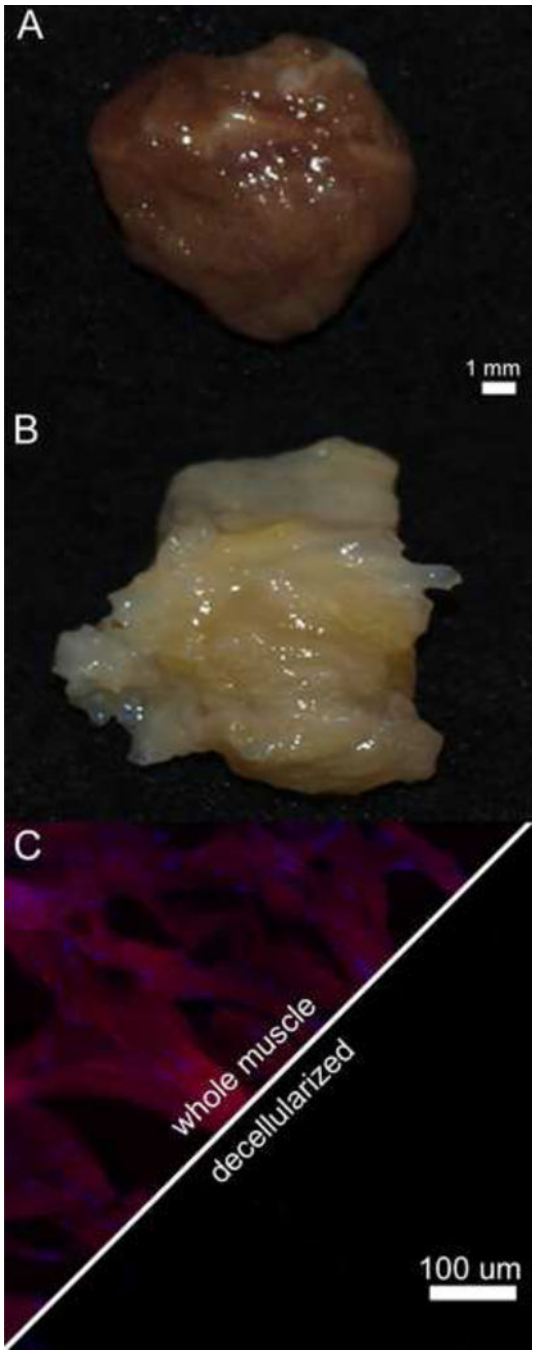

Figure 2:
Whole muscle tissue samples were characterized by a deep red color consistent with the presence of the intracellular iron-binding molecule myoglobin. Following decellularization treatment, myoglobin was no longer visualized and samples had transitioned to an off white color. When viewed microscopically, whole muscle tissue samples (C) were strongly reactive to molecules directed against actin (red) and nuclei (blue). Following decellularization actin and nuclei reactivity could not be detected in any of the samples tested.

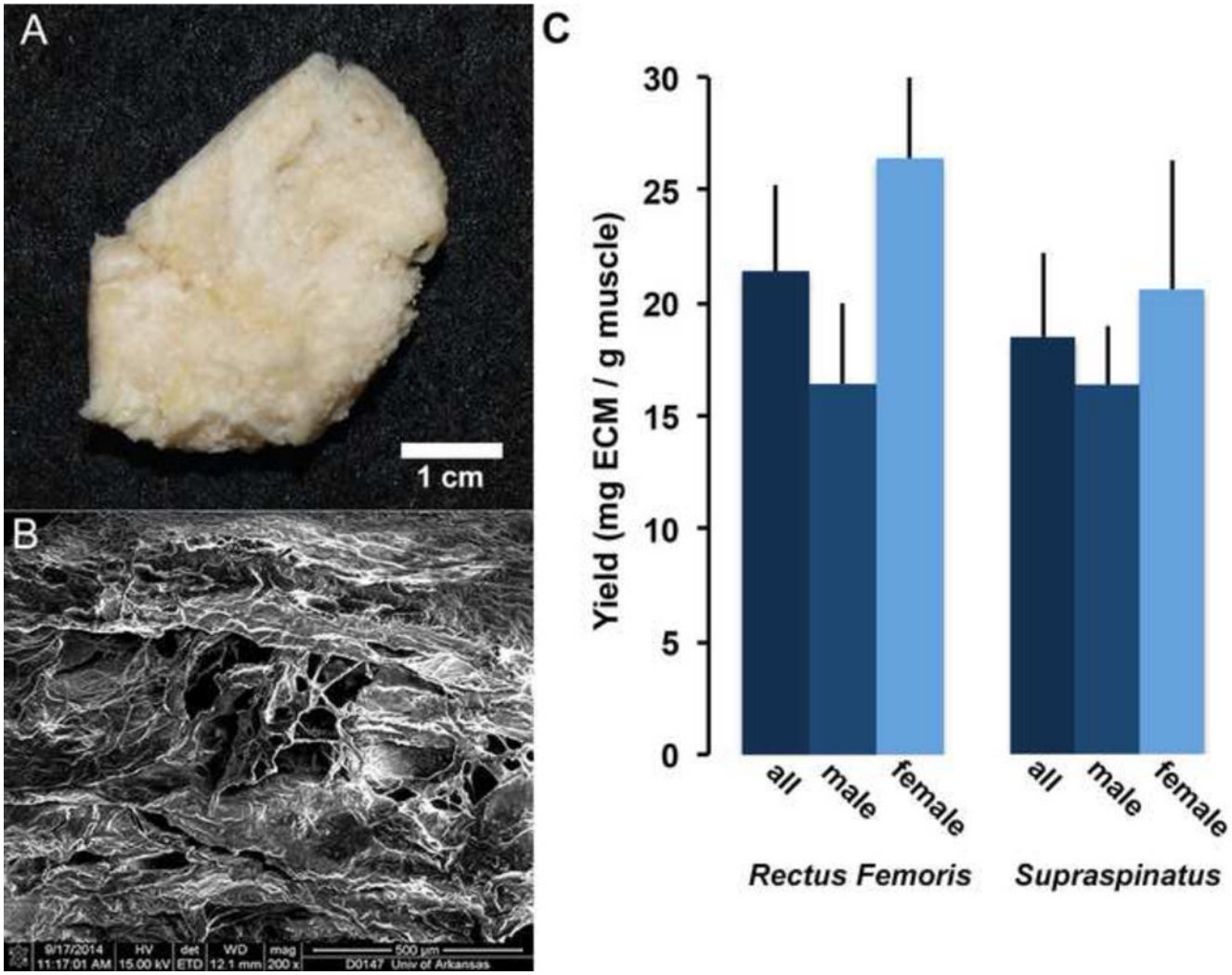

Figure 3:

Lyophilized bulk DSM samples viewed macroscopically (A) and in magnified SEM images (B) illustrate the surface architecture, porosity, and evidence of network alignment (left to right). On average, approximately 20 mg of DSM material was collected for each gram (wet weight) of whole muscle tissue (C).

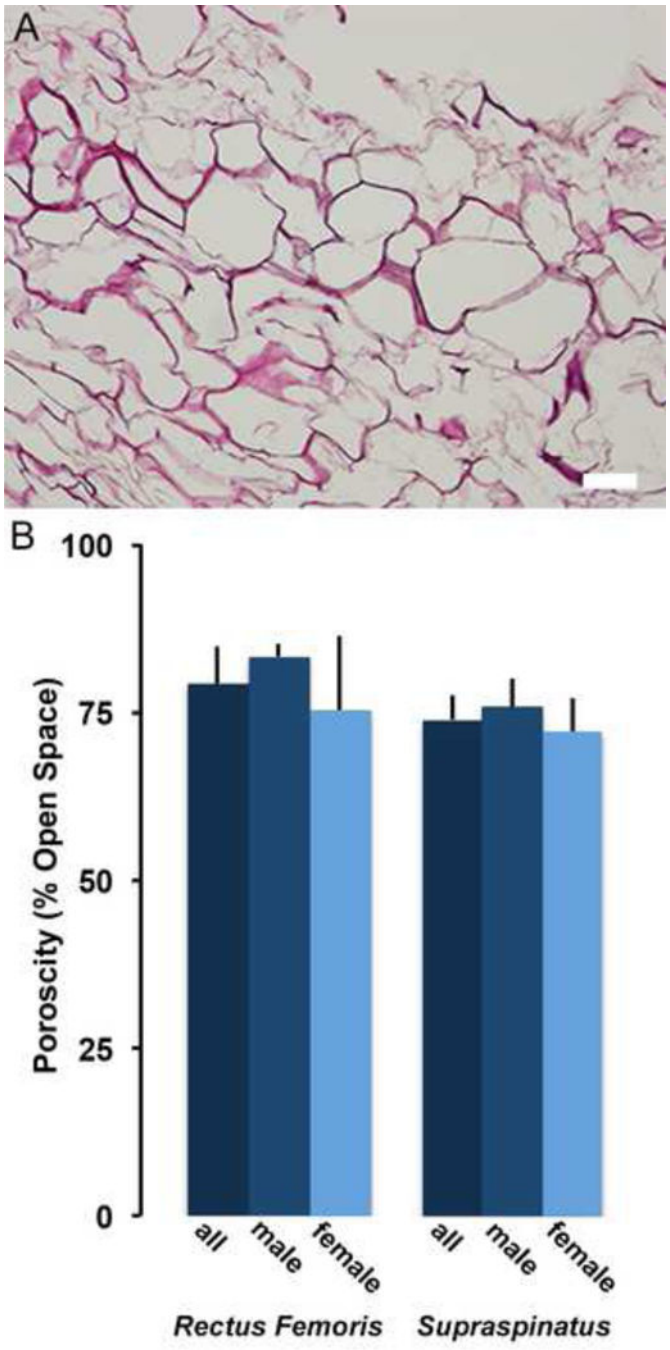

Figure 4:

Histological transverse thin sections (5um) were characterized by a porous yet interconnected network with circular pore structure (A). DSM sample porosity (average = 76.5 ± 3.2%) was consistent across muscle types and genders (B).

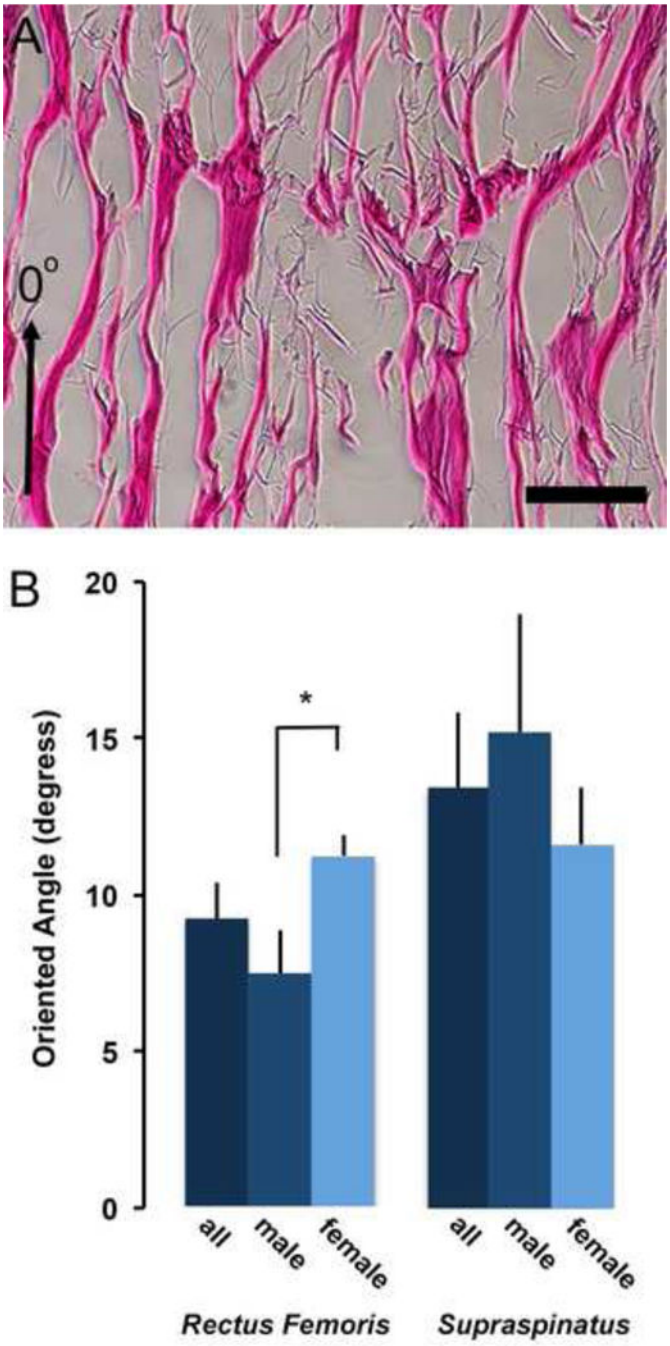

Figure 5:

Histological longitudinal thin sections (5um) of DSM samples were characterized by an aligned network of ECM material oriented in the direction of muscle contraction (arrow) Both rectus femoris and supraspinatus DSM samples showed similar levels of alignment, while within the rectus femoris samples there was a trend towards increased network alignment in female DSM samples (ANOVA; $p<0.05$)

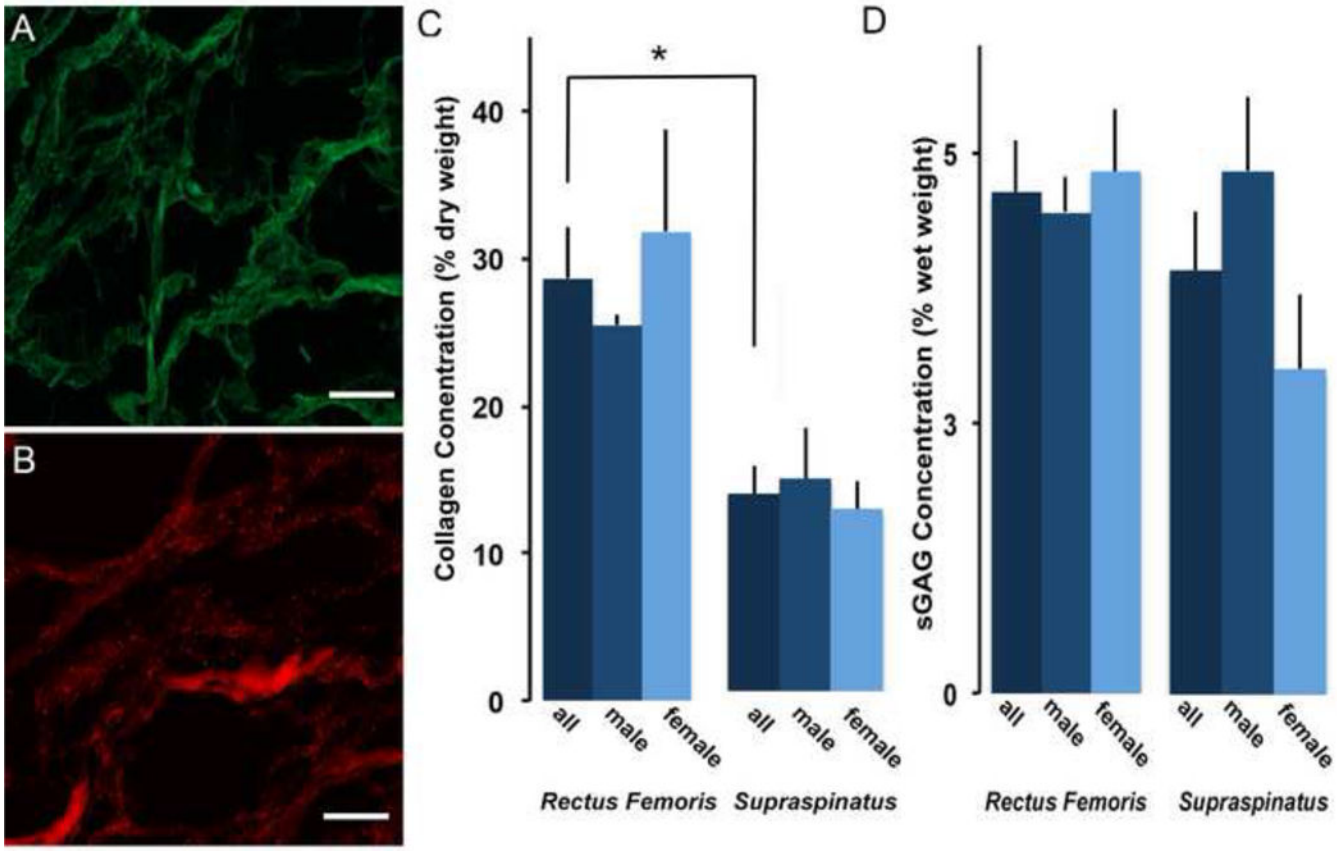

Figure 6:

DSM samples were immunostained to identify the presence of collagen type 1 (green) and CSPG (red). DSM samples, as seen with fluorescent illumination were immuno-reactive to both collagen type 1 (A) and CSPGs (B). The percent collagen content (dry weight) and sGAG content (wet weight) of DSM samples was estimated from hydroxy-proline (D) and dimethylmethylene blue concentration (C) measurements.

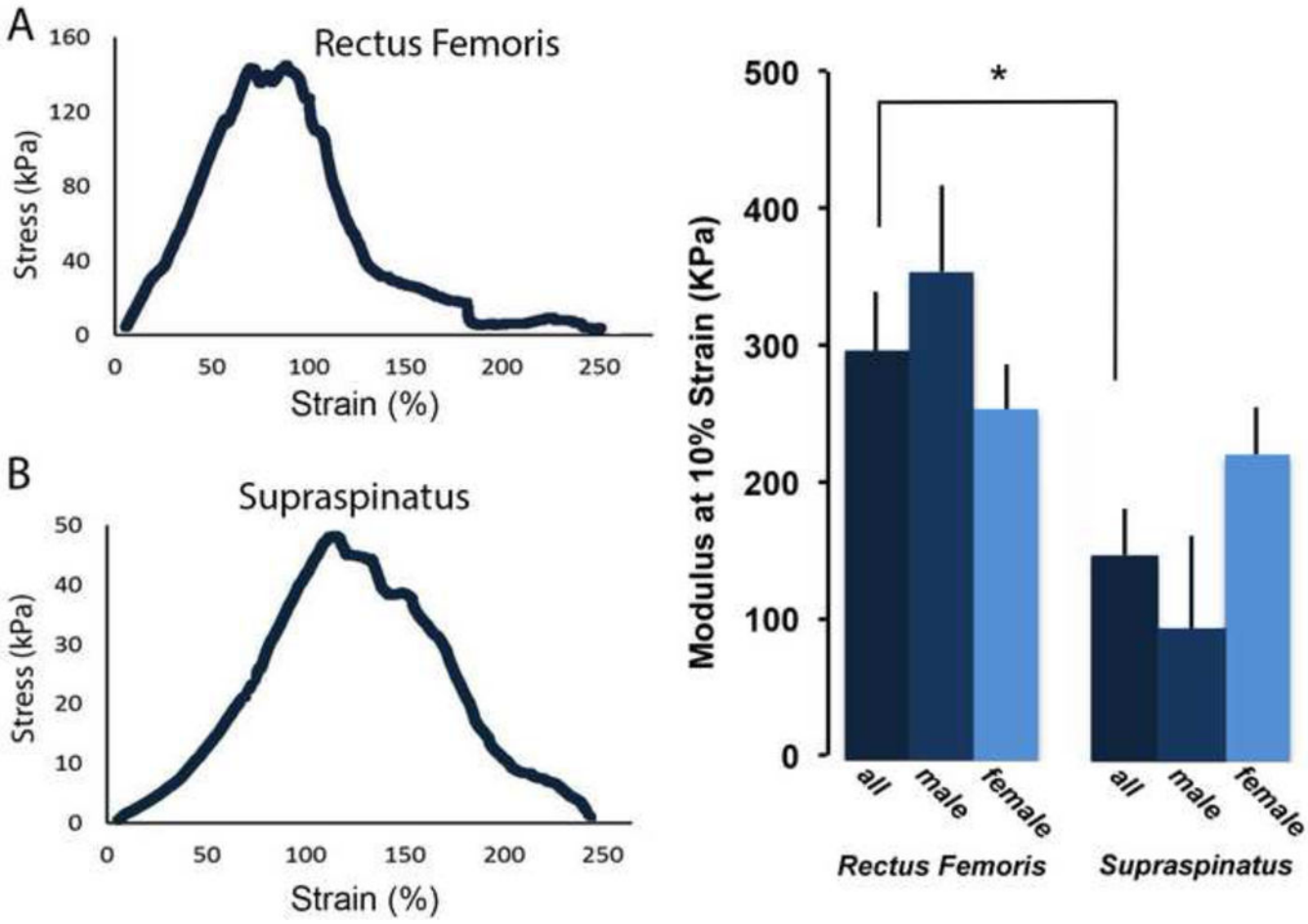

Figure 7:

Representative stress (kPa) vs. strain (%) curves for DSM samples prepared from rectus femoris (A) and supraspinatus muscle samples (B). Average modulus of elasticity (kPa) values were calculated at 10% strain for each of the samples tested. (* muscle location ANOVA $p<0.05$)

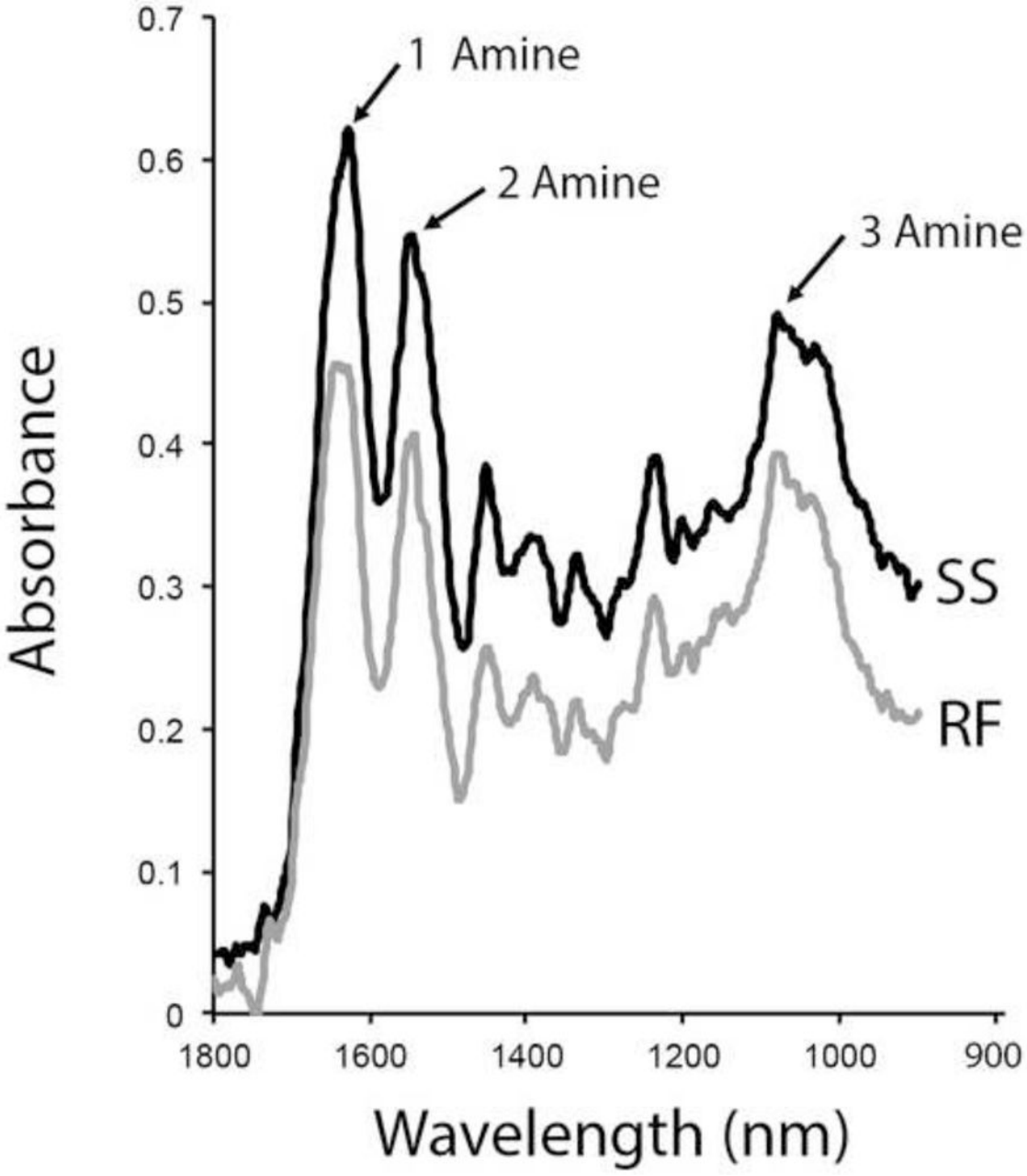

Figure 8:

Representative FTIR spectra collected from supraspinatus and rectus femoris DSM samples. Telltale amine peaks (open arrows) were observed within the FTIR spectra for both muscle types. No differences in the spectra were noted. Spectra are offset for clarity.

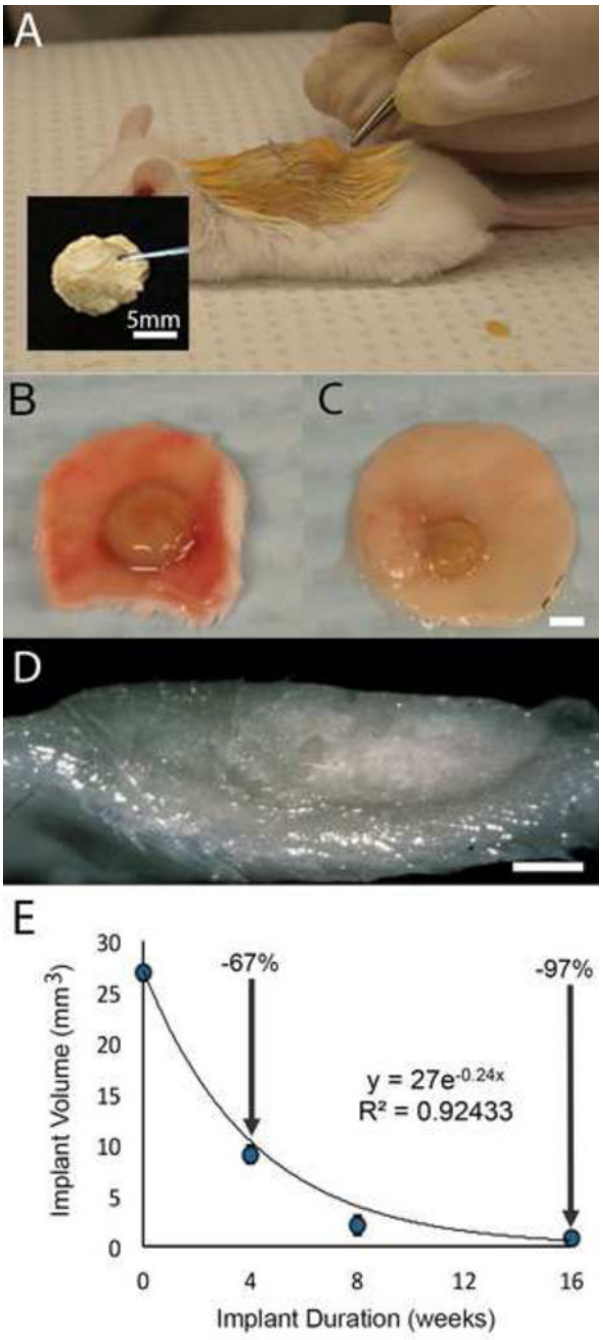

Figure 9:

DSM muscle pellets (A: inset) were subcutaneously implanted into outbred male mice (A). DSM implants and surrounding tissue were harvested at 4, 8, and 16 weeks (n=4 / time point). Measurements taken from microscopic images (B, C, and D) were used to calculate residual muscle pellet volume at each time point. Pellet degradation was modeled by an exponential decay curve fit (E), which was used to calculate biodegradation half-life (2.9 weeks).

Table 1:

Human Skeletal Muscle Donor Demographics (mean ± SEM)

	Rectus Femoris	Supraspinatus	All
Age (years)			
Male	74.6 ±7.6 (n=5)	66.2 ± 12.4 (n=5)	65.6± 5.8 (n=10)
Female	65.4 ± 7.9 (n=5)	65.4 ± 9.0 (n=5)	74.0± 6.0 (n=10)
Height (m)			
Male	1.77 ± 0.03	1.84 ± 0.13	1.80 ± 0.03
Female	1.60 ± 0.04	1.67 ± 0.07	1.62 ± 0.02
BMI (m/kg^2)			
Male	20.3 ± 3.1	17.6 ± 1.5	19.1 ± 1.5
Female	19.7 ± 2.5	22.4 ± 3.7	20.8 ± 1.7

Table 2:

Summary of skeletal muscle ECM material properties (Average, SEM, and range)

Material Property	Value (Mean ± SEM)	Range
ECM Yield (mg / g wet weight)	20.3 ± 2.6	8.0 – 39.8
Collagen Content (% dry weight)	21.1 ± 3.5	9.3 – 32.9
sGAG Content (% wet weight)	4.3 ± 0.3	2.1 – 5.7
Porosity (% open space)	76.5 ± 3.2	43.3 – 88.0
Oriented Angle (degrees)	12 ± 1.5	5.9 – 15.7
Modulus at 10% Strain (kPa)	218 ± 40.8	44.8 – 432.8
Half Life (Weeks)	2.9	NA